Research Article | Vol. 9, No. 10 | 1 Oct 2018 | BIOMEDICAL OPTICS EXPRESS 4792
Biomedical Optics EXPRESS

Establishing the quantitative relationship between diffuse speckle contrast analysis signals with absolute blood flow

JIALIN LIU,[1] HAIYANG WANG,[1] PEIPEI WANG,[1] ZHILIANG JIN,[1] WEIMIN LI,[1] HONGCHAO ZHANG,[2] ZHONGHUA SHEN,[2] AND DAXI XIONG[1,*]

[1]*Suzhou Institute of Biomedical Engineering and Technology, Chinese Academy of Sciences, No. 88 Keling Street, Suzhou 215163, China*
[2]*School of Science, Nanjing University of Science and Technology, No. 200 Xiaolingwei Street, Nanjing 210094, China*
**xiongdx@sibet.ac.cn*

Abstract: Diffuse speckle contrast analysis (DSCA) measures blood flow in deep tissues by taking advantage of the sensitivity of the speckle contrast signal to red blood cells (RBCs) motions. However, there has yet to be presented a clearly defined relationship between the absolute blood flow BF_{abs} and the measured speckle contrast signal. Here, we derive an expression of linear approximation function for speckle contrast, taking into account both shear-induced diffusive and correlated advective RBCs motions in the vessels. We provide a linear relationship between the slope k_{slope} of this linear function and BF_{abs}. The feasibility of this relationship is validated by Monte Carlo simulations of heterogeneous tissue with varying vessel radii. Furthermore, based on this quantitative relationship, we can determine the relative contributions of diffusive RBCs motion on the reduction of speckle contrast, considering different vascular morphology and flow profiles.

1. Introduction

Several optical approaches have been used for non-invasive blood flow measurements for the last several decades, in either single or multiple scattering regimes. The former technique, known as laser speckle contrast imaging (LSCI) [1–4], uses the spatio-temporal blurring of the speckle imaging defined as speckle contrast K to measure blood flow information in superficial tissues. LSCI is performed by the illumination of the biological tissue with a coherent light source and imaging of the reflected speckle by a camera. This technique allows the use of a simple experimental setup with the advantages of a relatively high spatio-temporal resolution, but under the condition of single or few scattering events it limits the photon penetration depth in the tissue [5].

On the other hand, diffuse correlation spectroscopy (DCS) [6, 7] has been developed for probing deep tissue blood flow by monitoring the light intensity fluctuations of the reflected diffuse speckle from the tissue. DCS offers continuous blood flow monitoring and has been extensively used for various clinical applications such as brain [8–10], cancer [11, 12] and muscle [13, 14]. Usually, DCS needs the single mode fiber with a smaller diameter, single photon counting avalanche photodiode and photon correlator to detect an independent speckle. To obtain a higher signal-to-noise (SNR), it is necessary to use multiple detectors to simultaneously acquire multiple independent speckles, which results in the increasing of the cost and complexity of DCS.

Recently, an alternative method called diffuse speckle contrast analysis (DSCA) [15–18] was developed for measuring blood flow in the deep tissue by the combination of LSCI and DCS. DSCA holds deep tissue probing capabilities of DCS and simple hardware instrument of LSCI. Generally, DSCA utilizes the dependence of measured speckle contrasts on source-detector distances or exposure time [19] to decouple the effects of absorption and scattering

#337760 https://doi.org/10.1364/BOE.9.004792
Journal © 2018 Received 2 Jul 2018; revised 15 Aug 2018; accepted 6 Sep 2018; published 12 Sep 2018

Biomedical Optics EXPRESS

[20, 21] from the dynamics, and, therefore, extracts a quantitative estimate of blood flow *in vivo* [22]. Besides, the fast cameras with a high frame rate [23, 24] can rapidly improve acquisition speed of speckle images.

In fact, DSCA and DCS are examining different aspects of the same entity [25], i.e., the temporal electric autocorrelation function of the diffusely reflected speckles caused by the movement of red blood cells (RBCs). Currently, the most common model for describing the RBCs motion is a Brownian diffusion-like process, which provides a better characterization of the autocorrelation function signals in a range of subjects and tissue types than the expected random flow model which describes the RBCs motion is ballistic. Based on Brownian motion model, we have developed and tested a thorough speckle contrast model [26–28] in DSCA for quantitative measurement of the RBCs motion. Although the blood flow index (BFI) in Brownian motion model has been shown to be approximately proportional to absolute blood flow BF_{abs}, the interpretation of the BFI is complicated due to its units of cm^2/s and the value of this proportionality between BFI and BF_{abs} is not clear in DSCA. Therefore, establishing the quantitative relationship between BFI in DSCA and BF_{abs} is urgently necessary and significant.

For this quantification, firstly it is necessary to clearly understand intravascular RBCs dynamics in the tissues. It has been found [29, 30] that RBCs undergo shear-induced displacement in blood flow, and the calculated electric autocorrelation function largely depends on this shear-induced diffusive RBCs motions, while the effect of correlated advective RBCs motion is relatively smaller [31–33]. The challenge of understanding the effect of diffusive and advective RBCs motions on DSCA signals stems from the fact that the speckle contrast signal is obtained from dynamic scattering inside the vessels and the vessels comprise only a small fraction of the tissue volume. Therefore, it is necessary to separate the intravascular scattering events from the extravascular scattering, and explicitly record the location of each dynamic scattering event in the vessels. Monte Carlo simulation [5, 31] can accurately model dynamic scattering event in the realistic and complex tissue.

In this paper, the reduction in speckle contrast due to the relative contribution of diffusive and correlated advective RBCs motions is studied by theory and Monte Carlo simulations. We derive the linear approximation expression for speckle contrast in the heterogeneous tissue with varying vessel radii and blood flow profiles, and establish the quantitative relationship between the slope k_{slope} of this linear function with the absolute blood flow BF_{abs}. Meanwhile, we employ three-dimensional Monte Carlo simulations of photons propagation through tissues to support these results. This linear approximation expression can be also used to model the speckle contrast signals in the realistic tissue with the heterogeneous blood flow profiles and a complex vascular network.

2. Theory and methods

2.1 Intravascular red blood cell motion

The question of the proper statistical model for describing intravascular RBCs motion and ultimately relating this model to the measured electric autocorrelation function or speckle contrast have been the subject of numerous studies [30, 34–36]. Usually, RBCs displacement has been modeled as random flow with $<\Delta r^2(\tau)> = V^2\tau^2$, where $<\Delta r^2(\tau)>$ is the mean-squared displacement (MSD) of RBCs in time τ and V^2 is the second moment of the velocity of RBCs, or as Brownian motion with $<\Delta r^2(\tau)> = 6D_B\tau$, where D_B is the effective Brownian diffusion coefficient. Unexpectedly, Brownian motion model leads to better description of the experimental results in validation studies compared with random flow model.

It should be noted that both models mentioned above have generally assumed that the dynamic scattering events with RBCs in vessels are uncorrelated. This assumption is valid if the photons scatter only once inside a vessel and then encounter another vessel before their direction becomes randomized by the scattering from extravascular tissue. In fact, the scattering length of the photons inside the vessel at the common laser wavelengths (790-

Biomedical Optics EXPRESS

810nm) used in DCS or DSCA is ~12μm [37], which is smaller than some vessel diameters in the tissue. This leads to the breakdown of this uncorrelated scattering assumption because the photons in a large vessel will most likely undergo multiple scattering events which are in fact highly correlated. When multiple scattering in a single vessel is present, the contribution of each scattering event to dynamic information depends on the velocity difference between subsequent correlated scattering events [38].

To account for the effect of correlated RBCs motions on the speckle contrast signal, it is necessary to understand RBCs dynamic in the vessels. Usually the spatial flow speed profile of the vessels has the form as [39]

$$v(r) = v_{\max}\left[1 - a\frac{r^m}{R^m}\right], \tag{1}$$

where v_{max} is the maximum speed at the center line of the vessel, R is the radius of the vessel, r is the distance from the vessel center line, a is a scale factor that determine the nonzero velocity at the vessel wall, and m is the bluntness of flow profile.

Equation (1) describes a general form of advective flow in vessels and is experimentally verified by the method of dynamic light scattering – optical coherence tomography (DLS-OCT) [33]. Usually, the flow profile of bigger vessels (R>20μm) [33] can be considered to be parabolic (i.e., m = 2) and there is more bluntness in smaller vessels. Meanwhile, recent studies [31, 32] found that in addition to advective motions RBCs also undergo shear-induced diffusive motions in the vessels. The shear-induced diffusion coefficient $D(r)$ is proportional to the shear rate α_{ss} [40], i.e.,

$$D(r) = \alpha_{ss}\left|\frac{\partial v(r)}{\partial r}\right| = \alpha_{ss}\frac{mav_{\max}r^{m-1}}{R^m}, \tag{2}$$

where α_{ss} has a magnitude of ~0.1 to 0.5 × 10^{-6}mm^2 [33].

Based on Eq. (1) and (2), we can determine the velocity of the location of each scattering event in the vessel taking into account both diffusive and advective RBCs motions. In the following section, we will show the effect of correlated RBC motion on electric autocorrelation function and speckle contrast.

2.2 Diffuse speckle contrast analysis (DSCA)

A speckle pattern is a random interference pattern generated when photons from coherent light are scattered in a random medium. If the scatterers in the medium are mobile, as in the case of RBCs, the time integrated speckle pattern recorded by the camera becomes blurred. DSCA qualifies this degree of blurring by the ratio of the measured standard variance (σ_I) to the mean intensity (μ_I) in spatial or temporal domain, as

$$K(\rho,T) = \frac{\sigma_I(\rho,T)}{\mu_I(\rho,T)}, \tag{3}$$

where ρ is the source-detector (SD) separation, T is the exposure time of the camera, and K is the speckle contrast. In fact, the speckle contrast is essentially related to the normalized electric autocorrelation function $g_1(r,\tau)$ [15, 16] as

$$K^2(\rho,T) = \frac{2\beta}{T}\int_0^T (1-\tau/T)\left[g_1(\rho,\tau)\right]^2 d\tau, \tag{4}$$

where β is a constant determined by the experimental setup [41], $g_1(\rho,\tau) = G_1(\rho,\tau)/G_1(\rho,0)$, $G_1(\rho,\tau) = \langle E(\rho,t)E^*(\rho,t+\tau)\rangle$, τ is the delay time and $E(\rho,t)$ is the light electric field.

Biomedical Optics EXPRESS

Formally, the transport of $G_1(\rho,\tau)$ in multiple scattering media is well modeled by the correlation diffusion equation (CDE) [7, 42]. Sakadžić et al. [32] recently considered the effect of the correlated RBCs motion with diffusive and advective dynamics on the CDE, and derived the expression of $G_1(\rho,\tau)$ in a realistic vascular network with a heterogeneous distribution of the vessels with different radii and flow velocities. For simplicity, we consider only one vessel type with the same radius R and blood flow in the tissue and the analytic solution of $G_1(\rho,\tau)$ for the semi-infinite media is given by [32]

$$G_1(\rho,\tau)=\frac{3\mu_s'}{4\pi}\left[\frac{\exp\left(-\kappa(\tau)r_1\right)}{r_1}-\frac{\exp\left(-\kappa(\tau)r_2\right)}{r_2}\right], \tag{5}$$

where

$$\kappa(\tau)=\sqrt{3\mu_a\mu_s'+\frac{3}{2}\mu_s'F(\tau)}, \tag{6}$$

$$F(\tau)=k_0^2 l_{\mathrm{tr}}^{-1}\delta_{\mathrm{ves}}\left(4D_{\mathrm{av}}\tau+\frac{2}{3}v_{\mathrm{av}}^2\tau^2\right). \tag{7}$$

Here, $r_1^2=\rho^2+z_0^2$, $r_2^2=\rho^2+\left(z_0+2z_{\mathrm{b}}\right)^2$, $z_{\mathrm{b}}=2\left(1-R_{\mathrm{eff}}\right)/\left[3\mu_s'\left(1+R_{\mathrm{eff}}\right)\right]$, $z_0=1/\mu_s'$, R_{eff} is the effective reflection coefficient accounting for the index mismatch between the tissue and surrounding medium [43], μ_a is the average absorption coefficient, μ_s' is the average reduced scattering coefficient, k_0 is the wavenumber of light in the media, l_{tr} is the mean free path in the vessel, δ_{ves} accounts for the probability of the dynamic scattering from RBCs. Note that the average optical properties (μ_a and μ_s') consider the heterogeneity of the tissue and can be measured by multi-distance DCS [44, 45] or frequency-domain spatially resolved spectroscopy [46]. Besides, the parameter δ_{ves} is currently difficult to determine experimentally and usually is estimated by the volume fraction of the vessels in the tissue. D_{av} and v_{av} are the average value of diffusion coefficient $D(r)$ and advective motion $v(r)$, respectively. This allows us to write [32]

$$D_{\mathrm{av}}=\frac{2}{R^2}\int_0^R D(r)rdr=\frac{2m\alpha_{\mathrm{ss}}a}{(m+1)R}v_{\max}, \tag{8}$$

$$v_{\mathrm{av}}=\frac{2}{R^2}\int_0^R v(r)rdr=\left(1-\frac{2a}{m+2}\right)v_{\max}. \tag{9}$$

Based on Eq. (4)-(9), we can determine the theoretical dependence of speckle contrast on the SD separation or exposure time under the condition of the combination of diffusive and convective RBCs motion. Meanwhile, we note that it is difficult to obtain the analytical expression for the speckle contrast function due to the complex computation process of integral equation, and the necessary steps to be taken to overcome it.

2.3 Linear approximation for diffuse speckle contrast analysis

Our previous works [27] have demonstrated that the relation between $1/K^2$ and exposure time can be described by a linear approximation equation and the slope k_{slope} is equal to the inverse of the correlation time (τ_c) of autocorrelation function $g_1(\rho,\tau)$. In this section, we derive the expressions for the correlation time τ_c and this linear approximation model considering diffusive and advective motion.

To obtain correlation time in Eq. (5), we firstly note that the function $G_1(\rho,\tau)$ is derived from the radiative transfer equation using diffusion approximation. Since diffusion

Biomedical Optics EXPRESS

approximation is usually valid when the SD separation ρ is much larger than the transport mean-free path z_0, r_2 in Eq. (5) can be approximately given by

$$r_2 = \left[r_1^2 + 2z_1^2\right]^{1/2} \approx r_1 + \frac{z_1^2}{r_1}, \quad \frac{1}{r_2} \approx \frac{1}{r_1}\left(1 - \frac{z_1^2}{r_1^2}\right), \tag{10}$$

where $z_1^2 = 2z_b\left(z_b + z_0\right)$ and $z_1 \ll r_1$. Thus, Eq. (5) can be approximated as

$$G_1(\rho,\tau) = \frac{3\mu_s' \exp\left[-\kappa(\tau) r_1\right]}{4\pi r_1}\left\{1 - \exp\left[-\frac{\kappa(\tau) z_1^2}{r_1}\right]\left(1 - \frac{z_1^2}{r_1^2}\right)\right\}. \tag{11}$$

Meanwhile, we can introduce another approximation $\exp\left[-\kappa(\tau_c) z_1^2 / r_1\right] \approx 1 - \kappa(\tau_c) z_1^2 / r_1$ when $\kappa(\tau_c) z_1^2 / r_1 \ll 1$, which is usually satisfied at the larger SD separation. This procedure yields the expression for $G_1(\rho,\tau_c)$

$$G_1(\rho,\tau_c) = \frac{3\mu_s' z_0^2}{4\pi r_1^2} \exp\left[-\kappa(\tau_c) r_1\right]\left[\kappa(\tau_c) + \frac{1}{r_1}\right]. \tag{12}$$

So $g_1(\rho,\tau_c)$ can be expressed as

$$g_1(\rho,\tau_c) = \frac{G_1(\rho,\tau_c)}{G_1(\rho,0)} = \frac{\left[r_1\kappa(\tau_c) + 1\right]\exp\left[-r_1\kappa(\tau_c)\right]}{\left(r_1\kappa_0 + 1\right)\exp\left(-r_1\kappa_0\right)}, \tag{13}$$

where $\kappa_0 = \sqrt{3\mu_a\mu_s'}$. Equation (13) can be subsequently written as

$$\ln\left[g_1(\rho,\tau_c)\right] = r_1\kappa_0 - \ln\left(r_1\kappa_0 + 1\right) + \ln\left[r_1\kappa(\tau_c) + 1\right] - r_1\kappa(\tau_c) = -1. \tag{14}$$

Thus, Eq. (14) can be further represented as

$$r_1\kappa(\tau_c) + 1 - \ln\left[r_1\kappa(\tau_c) + 1\right] = 2 + r_1\kappa_0 - \ln\left(r_1\kappa_0 + 1\right). \tag{15}$$

If we define $x = LnF(x_0)$ is the solution for the equation $x - \ln x = x_0$, this allows us to obtain the solution for Eq. (15) and write

$$\kappa(\tau_c) = \frac{LnF(\varepsilon_1) - 1}{r_1}, \tag{16}$$

where $\varepsilon_1 = 2 + r_1\kappa_0 - \ln\left(r_1\kappa_0 + 1\right)$, and ε_1 only depends on SD separation and optical properties of the tissue. Finally, the correlation time τ_c for $g_1(\rho,\tau)$ can be obtained from substitution of Eq. (6)-(9) into Eq. (16), i.e.,

$$\tau_c = \frac{\sqrt{\left[LnF(\varepsilon_1) - 1\right]^2 + r_1^2\varepsilon_2^2 - r_1^2\kappa_0^2} - r_1\varepsilon_2}{r_1 k_0 \sqrt{\mu_s' l_{tr}^{-1}\delta_{ves}}} \times \frac{1}{v_{av}}, \tag{17}$$

where

$$\varepsilon_2 = 3k_0\sqrt{\mu_s' l_{tr}\delta_{ves}}\,\frac{D_{av}}{v_{av}} = 3k_0\sqrt{\mu_s' l_{tr}^{-1}\delta_{ves}}\,\frac{2m\alpha_{ss}a}{(m+1)R}\left(1 - \frac{2a}{m+2}\right)^{-1}. \tag{18}$$

Equation (17) is a general result that determines the correlation time in DCS considering the combination of diffusive and advective RBCs motion. Meanwhile, we have demonstrated

Biomedical Optics EXPRESS

that the slope k_{slope} of the linear approximation model for DSCA is equal to the inverse of the correlation time [27], i.e., $k_{\text{slope}} = 1/\tau_c$. Thus, the corresponding speckle contrast $1/K^2$ can be approximatively expressed as

$$\frac{1}{K^2(\rho,T)} = \frac{1}{\beta}\left[\frac{r_1 k_0\sqrt{\mu_s' l_{\text{tr}}^{-1}\delta_{\text{ves}}}}{\sqrt{\left[LnF(\varepsilon_1)-1\right]^2 + r_1^2\varepsilon_2^2 - r_1^2\kappa_0^2} - r_1\varepsilon_2} v_{\text{av}}T + b_{\text{in}}\right], \tag{19}$$

where b_{in} is the intercept and can be obtained by the linear fitting.

In order to clearly understand the relationship between the blood flow index k_{slope} in Eq. (19) and absolute blood flow BF_{abs}, it is important to have a clear definition of BF_{abs} used in DCS and DSCA. Usually BF_{abs} is defined as the volume of blood transiting through a given cross-sectional area per second, which is given by cross-sectional area times average RBCs speed, i.e., $\text{BF}_{\text{abs}} = \pi R^2 v_{\text{av}}$. Therefore, a clear linear relationship between k_{slope} and BF_{abs} can be established by

$$k_{\text{slope}} = \frac{r_1 k_0\sqrt{\mu_s' l_{\text{tr}}^{-1}\delta_{\text{ves}}}}{\pi R^2\left\{\sqrt{\left[LnF(\varepsilon_1)-1\right]^2 + r_1^2\varepsilon_2^2 - r_1^2\kappa_0^2} - r_1\varepsilon_2\right\}}\text{BF}_{\text{abs}}. \tag{20}$$

From Eq. (20), it is apparent that the relative change in BF_{abs} can be rapidly obtained by calculating the corresponding change in k_{slope}. Meanwhile, knowledge of this proportionality in Eq. (20) is required to determine BF_{abs} form the measured k_{slope}. However, this proportionality is complicated and related to multiple parameters such as the vessel radius, RBCs rheology (a, m, and α_{ss}), optical properties of the tissue, δ_{ves} and SD separation, etc. Some parameters in tissue are now not accessible by experimental method and further studies are necessary to discuss this problem. Besides, an important assumption for deriving Eq. (20) is that the first order expansion $\exp\left[-\kappa(\tau_c)z_1^2/r_1\right] \approx 1-\kappa(\tau_c)z_1^2/r_1$ is a good approximation. In fact, this assumption is valid for the large SD separation, i.e., $\rho \gg 1/\mu_s'$. Analytical and numerical computations of the influence of this error due to this approximation on k_{slope} are given in the following section.

2.4 Monte Carlo simulation

For studying photon traversal inside the heterogeneous tissue and considering the effect of correlated RBCs motion on the speckle contrast, Monte Carlo simulation can be used to track the consecutive scattering events in the tissue. Our Monte Carlo code is based on a three dimensional voxelized model developed in Ref [47]. Each voxel of the Monte Carlo geometry is assigned the optical properties that determine the distribution of photon scattering lengths and the degree of the absorption. The Henyey-Greenstein phase function with corresponding anisotropy g [48, 49] within the voxel containing the scattering event is used to calculate the scattering angle.

The point source of photons with a defined direction is incident on the surface of the medium. The photons exiting the medium at different separations from the point source are detected. For each detected photon, the vector of momentum transfer $\vec{q}$ and the radial location of each scattering in different vessels, along with the absorption weight in the medium are saved. The momentum transfer $\vec{q}$ is defined as $\vec{q} = \vec{k}_s - \vec{k}_i$, where $\vec{k}_s$ and $\vec{k}_i$ are the scattered and incident field wavevector, respectively. $\vec{q}$ has a magnitude of $q = 2k_0\sin(\theta/2)$, where θ is the scattering angle of the photon. The saved radial positon of the scattering event is used to calculate advective and diffusive dynamics of RBCs by Eq. (1)

Biomedical Optics EXPRESS

and (2). Based on these recorded values, the correlation function $G_1(\rho,\tau)$ can be given by summing over all detected photons [31]

$$G_1(\rho,\tau)=\frac{1}{N_p}\sum_{n=1}^{N_p}\exp\left[-\frac{1}{2}\sum_{l=1}^{N_{v,n}}\left(\sum_{j=1}^{N_{s,n,l}}\vec{q}_{n,l,j}\cdot\vec{v}_{n,l,j}\right)^2\tau^2\right]$$
$$\times\exp\left(-\sum_{j=1}^{N_{s,n}}q_{n,j}^2D_{n,j}\tau\right)\exp\left(-\sum_{p=1}^{N_{\text{tis}}}\mu_{a,p}L_{n,p}\right), \quad (21)$$

where N_P is the number of photons detected at the specific SD separation, $N_{s,n}$ is the number of scattering event in $N_{v,n}$ vessels for the n'th detected photon, $N_{s,n,l}$ is the number of consecutive scattering events of the n'th detected photon in the l'th vessel, N_{tis} is the number of tissue type, $\mu_{a,p}$ is the absorption coefficient of the p'th tissue type, and $L_{n,p}$ is the total path length of the n'th detected photon in the p'th tissue type. Note that the sum $\left(\sum_{j=1}^{N_{s,n,l}}\vec{q}_{n,l,j}\cdot\vec{v}_{n,l,j}\right)^2$ is performed in the same vessel to consider the degree of correlation between $N_{s,n,l}$ consecutive scattering events. This equation considers the influence of RBCs displacements due to the correlated advective and diffusive motion on the decay of $G_1(\rho,\tau)$. Using Eq. (4) and the information about RBCs speed and shear-induced diffusion, we can further calculate the expected speckle contrast values by MC simulation.

3. MC simulation geometry and RBCs motion

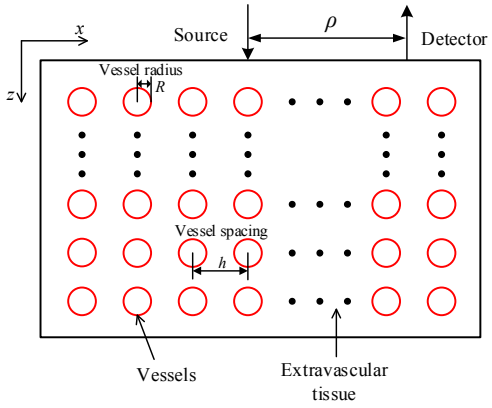

Fig. 1. (x, z) cross section of Monte Carlo simulation geometry.

To demonstrate the flexibility and validity of linear approximation model for DSCA in the heterogeneous media, a voxelized tissue-mimicking geometry in Fig. 1 is used in conjunction with Monte Carlo simulation to generate the speckle contrast measurements. Figure 1 shows the (x, z) cross section of the geometry with a size of 6 × 3cm. For simplicity, the blood vessels have the same radius R and are all oriented along the y-axis with an equal spacing h = 200μm [31] in x-axis and z-axis. The values of the radius R and the vessel spacing h determine the volume fraction of the vessels. If needed, other values for h can be further used to consider different volume fraction of the vessels. Therefore, the geometry has an infinite extent in y-axis due to the translation symmetry.

In our simulations, the blood flow profiles in Eq. (1) are assumed to be constant in time and approximately parabolic flow for the vessels with a larger radius (R>20μm), i.e., a = 1 and m = 2. In general, the vessels with a smaller radius tend to have a uniform flow profile and in this case RBCs motion is dominated by diffusive motion. Increasing the vessel radius

Biomedical Optics EXPRESS

and considering parabolic flow profiles can find the influence of correlated RBCs motion on speckle contrast signals. If needed, other values for a and m can be further used to consider different blood flow profiles in the future. Besides, the value of shear rate α_{ss} is set to 0.24×10^{-6}mm^2 from Ref [33]. measured in *vivo*.

For each simulation, 10^8 photons at a point are used to illuminate the surface of the geometry along z-axis and a 0.5mm × 0.5mm square region of interest (ROI) at different distances ρ from the source point is used as the detector. All of the information for calculating Eq. (21) and (4) are recorded by our MC simulation. Besides, the intravascular and extravascular optical properties at 800nm for a blood hematocrit 40% [37] are shown in Table 1.

Table 1. Optical properties for MC geometry

	μ_s (mm^{-1})	μ_a (mm^{-1})	g
Intravascular	82	0.3	0.977
Extravascular	10	0.002	0.9

4. Results

4.1 Corrected k_{slope} expression

Firstly, we test the accuracy of the expression for correlation time τ_c using theoretical data as shown in Fig. 2. An important assumption in this expression is that there are smaller errors arising from truncating SD separation terms in the Taylor Series expansion $\exp\left[-\kappa(\tau_c)z_1^2/r_1\right]$ to first order. This assumption is valid when using large SD separations ρ, i.e., $\rho \gg 1/\mu_s'$. Therefore, it is necessary to quantify the range of SD separation for which this expression can be accurately employed. The relative error in τ_c due to this assumption is defined as

$$\text{Error in } \tau_c = -\ln\left[g_1(\rho,\tau_c)\right]-1. \tag{22}$$

We control the fractional changes in all parameters used for the calculation of correlation time τ_c in Eq. (17) and isolate the influence of all parameters on the relative error in τ_c. The theoretical results show that the error in τ_c only depends on tissue optical properties (μ_a and μ_s') and SD separation, and the error signal is not sensitive to other parameters changes (such as v_{max}, a, m, etc.). As shown in Fig. 2, the change in relative error is greatest due to the combination term $\rho\mu_s'$ changes, and the changes in absorption μ_a and scattering μ_s' for the constant $\rho\mu_s'$ have the negligible influence on the relative error. Meanwhile, the error is relatively small (<5%) for the range $\rho\mu_s' \geq 10$.

In order to correct this error due to this assumption, the modified expression for correlation time τ_{cr} is introduced by

$$\tau_{cr} = \frac{\tau_c}{1+\text{Error in } \tau_c} = \frac{\tau_c}{-\ln\left[g_1(\rho,\tau_c)\right]}. \tag{23}$$

Note that knowledge of tissue optical properties (μ_a and μ_s') and SD separation can determine $\ln\left[g_1(\rho,\tau_{cr})\right]$ in Eq. (23).

Biomedical Optics EXPRESS

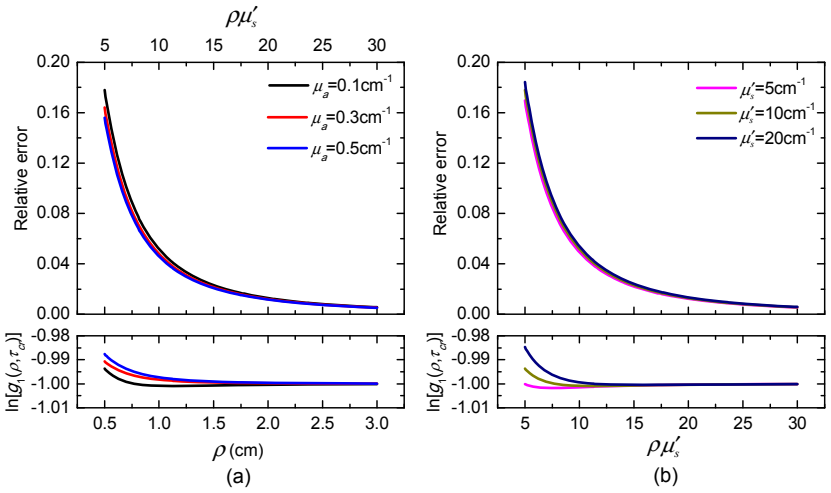

Fig. 2. Dependence of relative error in τ_c on (a) μ_a, (b) μ_s' and $\rho\mu_s'$, and corresponding corrected electric field autocorrelation function results $\ln\left[g_1(\rho,\tau_{cr})\right]$ at the modified correlation time τ_{cr}. Note that other parameters do not induce the change of the relative error. The change in relative error only depends on μ_a, μ_s' and SD separations.

Figure 2 also shows the corresponding corrected electric field autocorrelation function results $\ln\left[g_1(\rho,\tau_{cr})\right]$ at the modified correlation time τ_{cr}. We note that this error is relatively small and can be negligible, even for dimensionless term approaching $\rho\mu_s'=5$, which in turn implies higher accuracy and wider range for the modified τ_{cr} expression. Therefore, the corresponding expression for k_{slope} and BF_{abs} can be further corrected by Eq. (23)

$$k_{\text{slope}}=\frac{-\ln\left[g_1(\rho,\tau_c)\right]r_1k_0\sqrt{\mu_s'l_{\text{tr}}^{-1}\delta_{\text{ves}}}}{\pi R^2\left\{\sqrt{\left[LnF(\varepsilon_1)-1\right]^2+r_1^2\varepsilon_2^2-r_1^2\kappa_0^2}-r_1\varepsilon_2\right\}}\text{BF}_{\text{abs}}. \tag{24}$$

4.2 Validation with MC simulation data

In this section, we validate the linear approximation model by MC simulation results. We vary RBCs speed ($v_{\max}$ from 1mm/s to 6mm/s with a step of 1mm/s) and vessel radius (R = 20, 25, 30, 35, 40μm) with a fixed vessel spacing (h = 200μm) in MC simulations to test the dependence of k_{slope} on BF_{abs}. For all simulations, the intravascular and extravascular optical properties at 800nm for a blood hematocrit 40% are shown in Table 1. Then the average absorption μ_a and reduced scattering coefficients μ_s' of the mimicking tissue are given by the volume fraction weighted average of the intravascular ($\mu_{a,\text{in}}$ and $\mu_{s,\text{ex}}'$) and extravascular ($\mu_{a,\text{ex}}$ and $\mu_{s,\text{ex}}'$) optical coefficients, i.e., $\mu_a=\delta_{ves}\mu_{a,\text{in}}+(1-\delta_{ves})\mu_{a,\text{ex}}$ and $\mu_s'=\delta_{ves}\mu_{s,\text{in}}'+(1-\delta_{ves})\mu_{s,\text{ex}}'$, where $\delta_{ves}=\pi R^2/h^2$ is the volume fraction of blood vessel. Besides, the RBCs dynamics in vessels and other parameters are detailed in Sec. 3.

Biomedical Optics EXPRESS

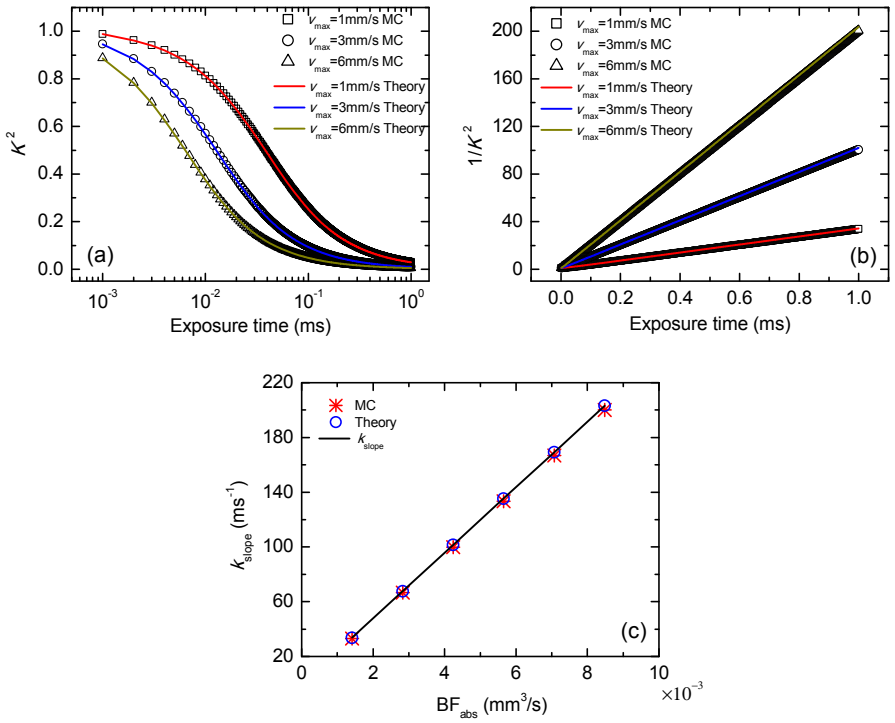

Fig. 3. MC simulation and theoretical results for (a) K^2 and (b) $1/K^2$ at different flow speeds v_{max}. The symbols and solid lines in (a) and (b) represent MC simulation and theoretical results, respectively. The symbols in (c) show the linear fitting results of k_{slope} versus BF_{abs}. The solid line in (c) is calculated by the corrected relation Eq. (24). Here, we use R = 30μm vessels and SD separation is 2cm.

Figure 3(a) and 3(b) show K^2 and $1/K^2$ results from MC simulations and theoretical calculations, respectively. In this example, the vessel radius is set to 30μm and SD separation is 2cm. Note that the theoretical results are numerically obtained by Eq. (4)-(9). These results show that the theoretical speckle contrast model fits MC simulation results well and the linear relation between $1/K^2$ and exposure time is obvious. Figure 3(c) shows the fitted values of k_{slope} versus BF_{abs}, compared with those calculated by the corrected relation using Eq. (24). These results in Fig. 3 demonstrate the validity of linear approximation model for DSCA and confirm that k_{slope} increases linearly with BF_{abs}.

Figure 4 shows the calculated absolute blood flow BF_{abs} from the linear fitting k_{slope} results at different SD separations. Note that the changes in the absolute blood flow BF_{abs} are accomplished by varying the vessel radius (from 20 to 40μm) with a fixed flow speed v_{max} = 3mm/s and vessel spacing h = 200μm. The solid lines in Fig. 4 represent the expected BF_{abs} results for SD separations of 1.0, 1.5 and 2.0cm. It is clearly found that this slope k_{slope} of the linear approximation model predict well the absolute blood flow BF_{abs}. The change in BF_{abs} can be simply obtained by calculating the change in k_{slope}.

Biomedical Optics EXPRESS

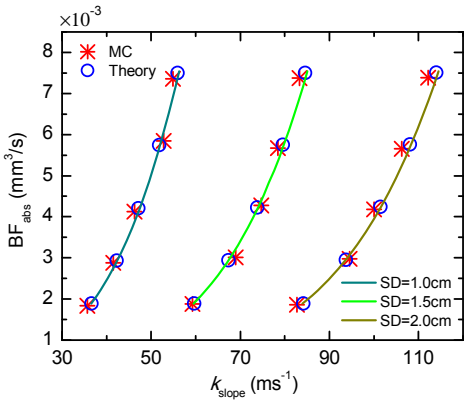

Fig. 4. Calculated BF_{abs} results for MC simulation and theoretical calculation versus linear fitting k_{slope} results. The solid lines at different SD separations are calculated by Eq. (24). The absolute blood flow BF_{abs} is accomplished by increasing the vessel radius from 20 to 40μm with a fixed flow speed v_{max} = 3mm/s and a fixed vessel spacing h = 200μm.

5. Discussion

Diffuse speckle contrast analysis (DSCA) has been employed extensively in blood flow measurement, in large part because of its simplicity. Usually the calculated speckle contrast fluctuations are driven by the RBCs motion and thus by blood flow. The question as to which model best characterizes RBCs motion within vessels has been widely studied. In this paper, we derive linear approximation expression for $1/K^2$ taking account both shear-induced diffusive and advective RBCs motions. To validate this theoretical model, we have performed Monte Carlo simulations in a simple tissue-mimicking geometry with parabolic flow profile and varying vessel radius. These theoretical and simulation results allow us to write a linear relation between the measured k_{slope} and absolute blood flow BF_{abs}. Meanwhile, in order to connect k_{slope} calculation to BF_{abs} some effects on this model need to be further discussed in actual applications.

It should be noted that our previous works [27] have deduced an analytical expression $k_{slope\text{-}DB}$ for diffusive RBCs motions, i.e.,

$$k_{slope\text{-}DB} = \frac{3\mu_s' l_{tr}^{-1} k_0^2 \delta_{ves} D_{av}}{4\chi}, \tag{25}$$

where

$$\chi = \left[\frac{3\mu_s'}{4\pi G_1(\rho,0)}\right]^2 \sum_{i=1}^{2}\sum_{j=1}^{2} \frac{(-1)^{i+j}}{2r_i r_j (r_i + r_j)^2}\left[1+\kappa_0(r_i+r_j)\right]\times e^{-\kappa_0(r_i+r_j)}. \tag{26}$$

It is worthwhile to determine the relative contribution of diffusive motion on k_{slope} in Eq. (24). We simply quantify this contribution by calculating the ratio between $k_{slope\text{-}DB}$ and k_{slope} as shown in Fig. 5. Here we have used a fixed vessel volume fraction δ_{ves} = 0.02, parabolic flow profile, a shear rate α_{ss} = 0.24 × 10^{-6}mm^2 and the same optical properties in Table 1. Figure 5 shows that increasing the vessel radius and decreasing SD separation both result in reduced importance of diffusive RBCs motion. Especially for the large vessel radius at the short SD separation [50], the advective RBCs motion may dominate k_{slope}. For the small vessel radius, k_{slope} mainly depends on diffusive RBCs motion. Furthermore, this contribution of diffusive motion also depends on other parameters of the vessels, such as shear rate α_{ss} and blood flow profile (a and m). So far the measured values of α_{ss} have large difference from in vivo and ex vivo [33, 40]. One can note that the higher the shear rate α_{ss}, the larger contribution of RBCs motion. The influence of blood flow profile on this contribution can be

Biomedical Optics EXPRESS

calculated by Eq. (24) and $k_{\text{slope-DB}}$. Equation (24) suggests an approach to determine the relative contributions of diffusive and advective RBCs motions on the reduction in speckle contrast.

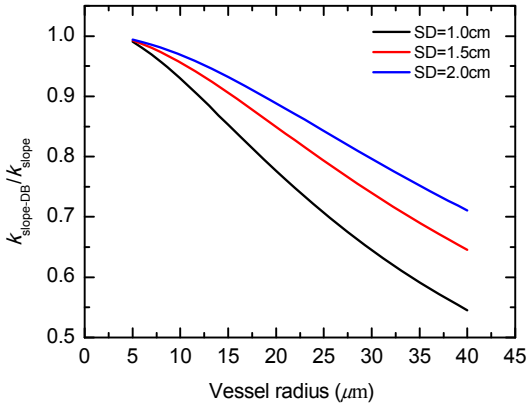

Fig. 5. Relative contributions of diffusive RBCs motions on the k_{slope} for different vessel radiuses and SD separations.

The source-detector (SD) separations used in MC simulation results are such that SD direction is perpendicular to the blood flow direction as shown in Fig. 1. In fact, the actual vessel directions in the tissue are random and complex. Figure 6(a) shows the effect of specific SD direction, which is perpendicular or parallel to vessel direction, and all used SD directions on the obtained speckle contrast $1/K^2$ results from the same MC simulations. It is obvious that the results $1/K^2$ tend to be the same and the corresponding absolute percentage changes in $1/K^2$ compared with the perpendicular case are shown in Fig. 6(b). The relative error in $1/K^2$ is no more than 2%. Meanwhile, Ref [31] have verified that the preferred direction of the vessels only introduce a small bias for the correlation function $g_1(\rho,\tau)$ compared with a truly random direction of the vessels. It is apparent that the calculated $1/K^2$ at a certain SD separation doesn't depend on the relative direction of SD separation with respect to vessel direction.

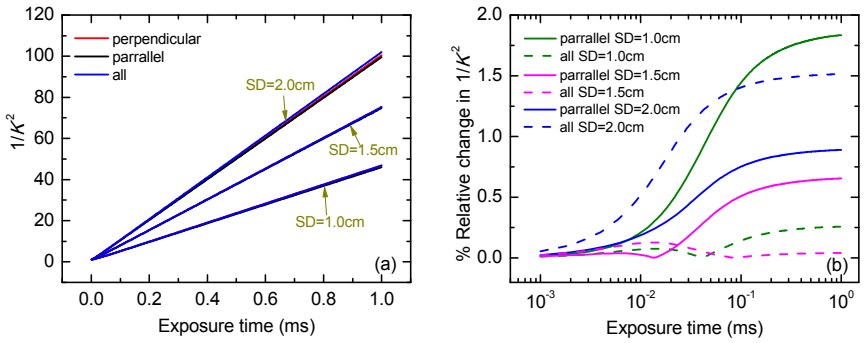

Fig. 6. Effect of SD direction with respect to vessel direction on the obtained speckle contrast $1/K^2$ results from MC simulations. The red and black lines in (a) indicate $1/K^2$ from SD separations that is perpendicular and parallel to vessel direction, respectively. The blue lines in (a) indicate $1/K^2$ from SD separations in all directions. The corresponding percentage change in $1/K^2$ at different SD separations compared with perpendicular case is shown in (b). Here, we use R = 30μm vessels with a fixed flow speed $v_{\max}$ = 3mm/s and a fixed vessel spacing h = 200μm.

For simplicity, we neglect the variation in radius and in flow speed among different vessels, and consider only one type of the vessel in this paper. In fact, when performing DSCA or DCS measurements in the tissue, the vessels encountered are different and

Biomedical Optics EXPRESS

complicated. For instance, capillaries with a small radius (<5μm) tend to be have similar velocities, but veins, venules, arterioles, and arteries all have different radii and flow speeds. Usually the photons come across multiple vessels along their path, each with different speeds and radiuses, and often interact with extravascular compartments. These contributions taken together cause the decay of speckle contrast function. Note that the analytic solutions for $G_1(\rho,\tau)$ [32] in Eq. (5)-(7) also can be used to predict DSCA signals in a realistic vascular network with a heterogeneous distribution of vessels with different radii and blood flow velocities. In this case, $F(\tau)$ in Eq. (7) can be expressed as [32]

$$F(\tau) = k_0^2 l_{\mathrm{tr}}^{-1} \int_{R_{\min}}^{R_{\max}} \int_{v_{\mathrm{ves,avmin}}}^{v_{\mathrm{ves,avmax}}} \delta_{\mathrm{ves}}\left[R, v_{\mathrm{ves,av}}(R)\right] dR\, dv_{\mathrm{ves,av}}(R) \times \left\{ 4D_{\mathrm{ves,av}}\left[R, v_{\mathrm{ves,av}}(R)\right]\tau + \frac{2}{3} v_{\mathrm{ves,av}}^2(R)\tau^2 \right\}, \quad (27)$$

where $\delta_{\mathrm{ves}}[R, v_{\mathrm{ves,av}}(R)]$ and $D_{\mathrm{ves,av}}[R, v_{\mathrm{ves,av}}(R)]$ are the volume fractions and average diffusion coefficient of the vessel with radius R and average velocity $v_{\mathrm{ves,av}}(R)$, respectively. Therefore, the average diffusion coefficient D_{av} and advective speed v_{av} in the linear approximation model have a complex nonlinear dependence on the distribution of vessel radius and RBCs speed distribution. It is important to point out that the differences of vessel radius and flow speed don't affect the validity of linear approximation model. This linear approximation expression can be used to model the speckle contrast signals in the realistic tissue with the heterogeneous blood flow profiles and a complex vessel geometry. Further measurements and numerical modeling of a realistic vascular network are needed to study the relation between the DSCA measurements and blood flow in the future.

Our results show that we can linearly relate the measured k_{slope} to absolute blood flow $\mathrm{BF_{abs}}$. Note that the proportionality is related to the vascular morphology, RBCs rheology, optical properties of the tissue, and SD separation. In order to accomplish the quantitative measurement of $\mathrm{BF_{abs}}$ from the measured k_{slope}, we need to have a detailed knowledge of these parameters. However, some parameters now are not readily accessible. But the progress in the experimental methods may make these parameters available in the future. Further research is needed to study the quantitative measurement of $\mathrm{BF_{abs}}$.

6. Conclusion

In summary, we have presented the theoretical derivations for linear approximation model in DSCA that consider both diffusive and correlated advective RBCs motion, and demonstrated that the slope k_{slope} of this linear model has a linear relation with absolute blood flow $\mathrm{BF_{abs}}$, which are in agreement with our Monte Carlo simulation results. Through this expression for k_{slope}, we can determine the relative contribution of diffusive motion on the reduction of speckle contrast. We expect further studies to use this relation to obtain a direct measurement of $\mathrm{BF_{abs}}$ in the more complex and realistic configurations of the tissue.

Funding

National Natural Science Foundation of China (NSFC) (11174151 and 11274175).

Disclosures

The authors declare that there are no conflicts of interest related to this article.

References

1. J. D. Briers and S. Webster, "Laser speckle contrast analysis (LASCA): a nonscanning, full-field technique for monitoring capillary blood flow," J. Biomed. Opt. **1**(2), 174–179 (1996).
2. D. A. Boas and A. K. Dunn, "Laser speckle contrast imaging in biomedical optics," J. Biomed. Opt. **15**(1), 011109 (2010).

Biomedical Optics EXPRESS

3. D. Briers, D. D. Duncan, E. Hirst, S. J. Kirkpatrick, M. Larsson, W. Steenbergen, T. Stromberg, and O. B. Thompson, "Laser speckle contrast imaging: theoretical and practical limitations," J. Biomed. Opt. **18**(6), 066018 (2013).
4. R. Bandyopadhyay, A. S. Gittings, S. S. Suh, P. K. Dixon, and D. J. Durian, "Speckle-visibility spectroscopy: a tool to study time-varying dynamics," Rev. Sci. Instrum. **76**(9), 093110 (2005).
5. M. A. Davis, S. M. Kazmi, and A. K. Dunn, "Imaging depth and multiple scattering in laser speckle contrast imaging," J. Biomed. Opt. **19**(8), 086001 (2014).
6. D. A. Boas, L. E. Campbell, and A. G. Yodh, "Scattering and imaging with diffusing temporal field correlations," Phys. Rev. Lett. **75**(9), 1855–1858 (1995).
7. D. A. Boas and A. G. Yodh, "Spatially varying dynamical properties of turbid media probed with diffusing temporal light correlation," J. Opt. Soc. Am. A **14**(1), 192–215 (1997).
8. C. Zhou, S. A. Eucker, T. Durduran, G. Yu, J. Ralston, S. H. Friess, R. N. Ichord, S. S. Margulies, and A. G. Yodh, "Diffuse optical monitoring of hemodynamic changes in piglet brain with closed head injury," J. Biomed. Opt. **14**(3), 034015 (2009).
9. M. N. Kim, T. Durduran, S. Frangos, B. L. Edlow, E. M. Buckley, H. E. Moss, C. Zhou, G. Yu, R. Choe, E. Maloney-Wilensky, R. L. Wolf, M. S. Grady, J. H. Greenberg, J. M. Levine, A. G. Yodh, J. A. Detre, and W. A. Kofke, "Noninvasive measurement of cerebral blood flow and blood oxygenation using near-infrared and diffuse correlation spectroscopies in critically brain-injured adults," Neurocrit. Care **12**(2), 173–180 (2010).
10. M. N. Kim, B. L. Edlow, T. Durduran, S. Frangos, R. C. Mesquita, J. M. Levine, J. H. Greenberg, A. G. Yodh, and J. A. Detre, "Continuous optical monitoring of cerebral hemodynamics during head-of-bed manipulation in brain-injured adults," Neurocrit. Care **20**(3), 443–453 (2014).
11. T. Durduran, R. Choe, G. Yu, C. Zhou, J. C. Tchou, B. J. Czerniecki, and A. G. Yodh, "Diffuse optical measurement of blood flow in breast tumors," Opt. Lett. **30**(21), 2915–2917 (2005).
12. G. Yu, "Near-infrared diffuse correlation spectroscopy in cancer diagnosis and therapy monitoring," J. Biomed. Opt. **17**(1), 010901 (2012).
13. Y. Shang, T. B. Symons, T. Durduran, A. G. Yodh, and G. Yu, "Effects of muscle fiber motion on diffuse correlation spectroscopy blood flow measurements during exercise," Biomed. Opt. Express **1**(2), 500–511 (2010).
14. G. Yu, Y. Shang, Y. Zhao, R. Cheng, L. Dong, and S. P. Saha, "Intraoperative evaluation of revascularization effect on ischemic muscle hemodynamics using near-infrared diffuse optical spectroscopies," J. Biomed. Opt. **16**(2), 027004 (2011).
15. R. Bi, J. Dong, and K. Lee, "Deep tissue flowmetry based on diffuse speckle contrast analysis," Opt. Lett. **38**(9), 1401–1403 (2013).
16. R. Bi, J. Dong, and K. Lee, "Multi-channel deep tissue flowmetry based on temporal diffuse speckle contrast analysis," Opt. Express **21**(19), 22854–22861 (2013).
17. C. Yeo, H. C. Park, K. Lee, and C. Song, "Avian embryo monitoring during incubation using multi-channel diffuse speckle contrast analysis," Biomed. Opt. Express **7**(1), 93–98 (2016).
18. M. Seong, Z. Phillips 5th, P. M. Mai, C. Yeo, C. Song, K. Lee, and J. G. Kim, "Simultaneous blood flow and blood oxygenation measurements using a combination of diffuse speckle contrast analysis and near-infrared spectroscopy," J. Biomed. Opt. **21**(2), 027001 (2016).
19. C. P. Valdes, H. M. Varma, A. K. Kristoffersen, T. Dragojevic, J. P. Culver, and T. Durduran, "Speckle contrast optical spectroscopy, a non-invasive, diffuse optical method for measuring microvascular blood flow in tissue," Biomed. Opt. Express **5**(8), 2769–2784 (2014).
20. Z. Hajjarian and S. K. Nadkarni, "Correction of optical absorption and scattering variations in Laser Speckle Rheology measurements," Opt. Express **22**(6), 6349–6361 (2014).
21. D. Irwin, L. Dong, Y. Shang, R. Cheng, M. Kudrimoti, S. D. Stevens, and G. Yu, "Influences of tissue absorption and scattering on diffuse correlation spectroscopy blood flow measurements," Biomed. Opt. Express **2**(7), 1969–1985 (2011).
22. T. Dragojević, J. L. Hollmann, D. Tamborini, D. Portaluppi, M. Buttafava, J. P. Culver, F. Villa, and T. Durduran, "Compact, multi-exposure speckle contrast optical spectroscopy (SCOS) device for measuring deep tissue blood flow," Biomed. Opt. Express **9**(1), 322–334 (2018).
23. S. Sun, B. R. Hayes-Gill, D. He, Y. Zhu, and S. P. Morgan, "Multi-exposure laser speckle contrast imaging using a high frame rate CMOS sensor with a field programmable gate array," Opt. Lett. **40**(20), 4587–4590 (2015).
24. T. Dragojević, D. Bronzi, H. M. Varma, C. P. Valdes, C. Castellvi, F. Villa, A. Tosi, C. Justicia, F. Zappa, and T. Durduran, "High-speed multi-exposure laser speckle contrast imaging with a single-photon counting camera," Biomed. Opt. Express **6**(8), 2865–2876 (2015).
25. R. Bi, J. Dong, C. L. Poh, and K. Lee, "Optical methods for blood perfusion measurement--theoretical comparison among four different modalities," J. Opt. Soc. Am. A **32**(5), 860–866 (2015).
26. J. Liu, H. Zhang, Z. Shen, J. Lu, and X. Ni, "Quantitatively assessing flow velocity by the slope of the inverse square of the contrast values versus camera exposure time," Opt. Express **22**(16), 19327–19336 (2014).
27. J. Liu, H. Zhang, J. Lu, X. Ni, and Z. Shen, "Quantitative model of diffuse speckle contrast analysis for flow measurement," J. Biomed. Opt. **22**(7), 076016 (2017).
28. J. Liu, H. Zhang, J. Lu, X. Ni, and Z. Shen, "Simultaneously extracting multiple parameters via multi-distance and multi-exposure diffuse speckle contrast analysis," Biomed. Opt. Express **8**(10), 4537–4550 (2017).

Biomedical Optics EXPRESS

29. S. A. Carp, N. Roche-Labarbe, M. A. Franceschini, V. J. Srinivasan, S. Sakadžić, and D. A. Boas, "Due to intravascular multiple sequential scattering, diffuse correlation spectroscopy of tissue primarily measures relative red blood cell motion within vessels," Biomed. Opt. Express **2**(7), 2047–2054 (2011).
30. M. Ninck, M. Untenberger, and T. Gisler, "Diffusing-wave spectroscopy with dynamic contrast variation: disentangling the effects of blood flow and extravascular tissue shearing on signals from deep tissue," Biomed. Opt. Express **1**(5), 1502–1513 (2010).
31. D. A. Boas, S. Sakadžić, J. Selb, P. Farzam, M. A. Franceschini, and S. A. Carp, "Establishing the diffuse correlation spectroscopy signal relationship with blood flow," Neurophotonics **3**(3), 031412 (2016).
32. S. Sakadžic, D. A. Boas, and S. Carp, "Theoretical model of blood flow measurement by diffuse correlation spectroscopy," J. Biomed. Opt. **22**(2), 027006 (2017).
33. J. Tang, S. E. Erdener, B. Li, B. Fu, S. Sakadžić, S. A. Carp, J. Lee, and D. A. Boas, "Shear-induced diffusion of red blood cells measured with dynamic light scattering-optical coherence tomography," J. Biophotonics **11**(2), e201700070 (2018).
34. K. Verdecchia, M. Diop, L. B. Morrison, T. Y. Lee, and K. St Lawrence, "Assessment of the best flow model to characterize diffuse correlation spectroscopy data acquired directly on the brain," Biomed. Opt. Express **6**(11), 4288–4301 (2015).
35. D. D. Duncan and S. J. Kirkpatrick, "Can laser speckle flowmetry be made a quantitative tool?" J. Opt. Soc. Am. A **25**(8), 2088–2094 (2008).
36. K. Khaksari and S. J. Kirkpatrick, "Laser speckle contrast imaging is sensitive to advective flux," J. Biomed. Opt. **21**(7), 76001 (2016).
37. M. Meinke, G. Müller, J. Helfmann, and M. Friebel, "Empirical model functions to calculate hematocrit-dependent optical properties of human blood," Appl. Opt. **46**(10), 1742–1753 (2007).
38. D. Bicout, E. Akkermans, and R. Maynard, "Dynamical correlations for multiple light scattering in laminar flow," J. Phys. **1**(4), 471–491 (1991).
39. G. J. Tangelder, D. W. Slaaf, A. M. Muijtjens, T. Arts, M. G. oude Egbrink, and R. S. Reneman, "Velocity profiles of blood platelets and red blood cells flowing in arterioles of the rabbit mesentery," Circ. Res. **59**(5), 505–514 (1986).
40. H. L. Goldsmith and J. C. Marlow, "Flow behavior of erythrocytes. II. Particle motions in concentrated suspensions of ghost cells," J. Colloid Interface Sci. **71**(2), 383–407 (1979).
41. P.-A. Lemieux and D. J. Durian, "Investigating non-Gaussian scattering processes by using nth-order intensity correlation functions," J. Opt. Soc. Am. A **16**(7), 1651–1664 (1999).
42. T. Durduran, R. Choe, W. B. Baker, and A. G. Yodh, "Diffuse optics for tissue monitoring and tomography," Rep. Prog. Phys. **73**(7), 076701 (2010).
43. R. C. Haskell, L. O. Svaasand, T. T. Tsay, T. C. Feng, M. S. McAdams, and B. J. Tromberg, "Boundary conditions for the diffusion equation in radiative transfer," J. Opt. Soc. Am. A **11**(10), 2727–2741 (1994).
44. P. Farzam and T. Durduran, "Multidistance diffuse correlation spectroscopy for simultaneous estimation of blood flow index and optical properties," J. Biomed. Opt. **20**(5), 055001 (2015).
45. D. Tamborini, P. Farzam, B. Zimmermann, K. C. Wu, D. A. Boas, and M. A. Franceschini, "Development and characterization of a multidistance and multiwavelength diffuse correlation spectroscopy system," Neurophotonics **5**(1), 011015 (2018).
46. D. Irwin, L. Dong, Y. Shang, R. Cheng, M. Kudrimoti, S. D. Stevens, and G. Yu, "Influences of tissue absorption and scattering on diffuse correlation spectroscopy blood flow measurements," Biomed. Opt. Express **2**(7), 1969–1985 (2011).
47. D. Boas, J. Culver, J. Stott, and A. Dunn, "Three dimensional Monte Carlo code for photon migration through complex heterogeneous media including the adult human head," Opt. Express **10**(3), 159–170 (2002).
48. S. A. Prahl, M. Keijzer, S. L. Jacques, and A. J. Welch, "A Monte Carlo model of light propagation in tissue," SPIE Proc. Dosim. Laser Radiat. Med. Biol. **1**, 102–111 (1989).
49. L. Wang, S. L. Jacques, and L. Zheng, "MCML-Monte Carlo modeling of light transport in multi-layered tissues," Comput. Methods Programs Biomed. **47**(2), 131–146 (1995).
50. S. M. S. Kazmi, E. Faraji, M. A. Davis, Y.-Y. Huang, X. J. Zhang, and A. K. Dunn, "Flux or speed? Examining speckle contrast imaging of vascular flows," Biomed. Opt. Express **6**(7), 2588–2608 (2015).